Native Ion Mobility-Mass Spectrometry Reveals the Formation of β-Barrel Shaped Amyloid-β Hexamers in a Membrane-Mimicking Environment

Nicklas Österlund,[†] Rani Moons,[‡] Leopold L. Ilag,[§] Frank Sobott,[*,‡,∥,⊥] and Astrid Gräslund[*,†]

[†]Department of Biochemistry and Biophysics, Stockholm University, Stockholm, Sweden

[‡]Department of Chemistry, University of Antwerp, Antwerp, Belgium

[§]Department of Environmental Science and Analytical Chemistry, Stockholm University, Stockholm, Sweden

[∥]The Astbury Centre for Structural Molecular Biology, University of Leeds, Leeds, The United Kingdom

[⊥]School of Molecular and Cellular Biology, University of Leeds, Leeds, The United Kingdom

S *Supporting Information*

ABSTRACT: The mechanisms behind the Amyloid-β (Aβ) peptide neurotoxicity in Alzheimer's disease are intensely studied and under debate. One suggested mechanism is that the peptides assemble in biological membranes to form β-barrel shaped oligomeric pores that induce cell leakage. Direct detection of such putative assemblies and their exact oligomeric states is however complicated by a high level of heterogeneity. The theory consequently remains controversial, and the actual formation of pore structures is disputed. We herein overcome the heterogeneity problem by employing a native mass spectrometry approach and demonstrate that Aβ(1−42) peptides form coclusters with membrane mimetic detergent micelles. The coclusters are gently ionized using nanoelectrospray and transferred into the mass spectrometer where the detergent molecules are stripped away using collisional activation. We show that Aβ(1−42) indeed oligomerizes over time in the micellar environment, forming hexamers with collision cross sections in agreement with a general β-barrel structure. We also show that such oligomers are maintained and even stabilized by addition of lipids. Aβ(1−40) on the other hand form significantly lower amounts of oligomers, which are also of lower oligomeric state compared to Aβ(1−42) oligomers. Our results thus support the oligomeric pore hypothesis as one important cell toxicity mechanism in Alzheimer's disease. The presented native mass spectrometry approach is a promising way to study such potentially very neurotoxic species and how they could be stabilized or destabilized by molecules of cellular or therapeutic relevance.
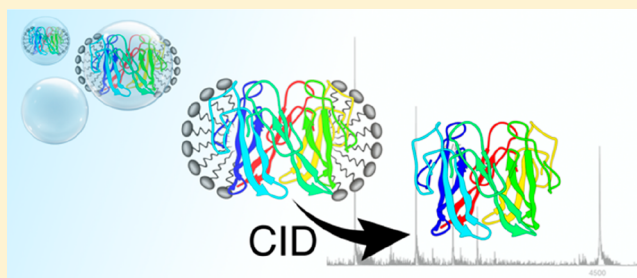
INTRODUCTION

The Amyloid-β (Aβ) peptide is a small (39−43 amino acids) amphiphilic peptide which is produced by proteolytic cleavage of an integral membrane protein, the Amyloid Precursor Protein (APP). The central and C-terminal parts of Aβ belong to a segment of the transmembrane domain of APP, while the Aβ N-terminal segment (residues 1−16) is found on the extracellular part of APP, outside the cell membrane.[1] The Aβ peptide aggregates spontaneously in aqueous solution, forming amyloid fibrils similar to those found in the brain of Alzheimer's disease (AD) patients. Aβ production, aggregation, and accumulation are therefore important hallmarks of AD pathology.[2] It has however been reported that AD pathology severity does not correlate well with the concentration of amyloid plaques. Instead the soluble pool of Aβ seems to be related to neurodegeneration.[3] It has been proposed that the small oligomeric forms of Aβ are the most neurotoxic species. One suggested mechanism for such toxicity is that a peptide oligomer inserts into the cellular membrane as a pore and induces cell leakage.[4,5] The longer Aβ(1−42) is also more neurotoxic than Aβ(1−40), which is more abundant in the cell. Significant differences between the two isoforms have furthermore been observed when it comes to primary nucleation rates for aggregation, oligomerization states, and interactions with membranes.[6−8]

Although the membrane disturbing properties of Aβ are well established, the exact molecular mechanisms remain elusive. The idea of pore forming oligomers is a highly controversial one and is challenged by several other theories. Other membrane damaging mechanisms which have some experimental evidence include mechanical disruption and/or extraction of lipids by growing fibril structures, as well as change of membrane curvature and/or thickness by mem-

brane—peptide interactions.[9−12] It is also highly probable that several of these mechanisms can occur simultaneously or sequentially during experimental conditions. A two-step mechanism for membrane disruption by Aβ has been proposed where ion selective pores are first formed, followed by general membrane fragmentation damage by growing amyloid fibrils.[13] A cellular membrane also has various physicochemical properties which could affect its interaction with Aβ, and also modulate the different toxicity mechanisms. Surface curvature and membrane thickness have for instance been shown to affect amyloid aggregation and toxicity.[14,15]

Due to the complexity of biological membranes, simpler membrane-like systems are often used for detailed studies of Aβ interactions with membranes. Several biochemical and biophysical techniques, as well as membrane mimetic systems are available to probe the interactions.[16] Detection of putative Aβ pore-structures is however challenging as the Aβ population is a heterogeneous mixture of different water-soluble and insoluble aggregates, both in solution and in membrane mimicking environments.[17,18] It should be noted that Aβ oligomers are generally not well-defined, and despite careful attempts their heterogeneous sizes and structures are not yet well characterized. Formation of both β-sheet structured and disordered oligomers have been demonstrated.[19,20] It has also been suggested that β-sheet structured and unstructured oligomers coexist as Aβ aggregation proceeds via two distinct pathways, with the β-sheet structured aggregates being the most neurotoxic.[21]

Recently a systematic study was published which outlined a reproducible protocol for preparation of small β-barrel pore-forming oligomers (βPFO) in membrane mimicking micelles.[22] It was found that Aβ(1−42), but not Aβ(1−40), formed such βPFOs and that zwitterionic dodecylphosphocholine (PC12, DPC) micelles yielded the highest amount of β-sheet structured oligomers (As seen by CD and NMR spectroscopy). The study showed that micelle-βPFO$_{Aβ(1−42)}$ cocomplexes of approximately 60 kDa were formed (determined by size exclusion chromatography) under such conditions. The exact size or size distribution of βPFO$_{Aβ(1−42)}$ without detergent was however not reported.

In the present study, we employ native mass spectrometry to detect the formation of specific Aβ oligomers in a membrane mimicking environment. Native mass spectrometry, i.e. the use of gentle conditions to retain specific noncovalent interactions in the gas phase, has emerged as a powerful tool in structural biology. Such use of mass spectrometry allows for rapid identification of complex stoichiometry, protein modifications, and binding of specific cofactors.[23] Mass spectrometry can also be coupled to ion mobility (IM) spectrometry which is a related gas phase technique that separates ions according to their collisional cross section (CCS, Ω). For proteins, such observations give information about both their conformations and about oligomeric states that overlap in the mass spectrometric m/z dimension. Native IM-MS has shown that Aβ(1−42) and Aβ(1−40) oligomers in solution differ significantly: Aβ(1−42) adopts an open tetramer structure leading to formation of higher oligomer states while Aβ(1−40) oligomerization stops at a closed tetramer.[6] However, oligomerization in a membrane-like environment has never been previously reported using native (IM-)MS.

The application of native mass spectrometry has been extended to study membrane proteins using membrane mimicking systems. Detergent micelles are most commonly used to stabilize membrane proteins, but lipid based models such as nanodiscs have also been successfully employed.[24−26] The intact protein-model membrane cocluster is ionized under gentle electrospray conditions, whereafter the protein is liberated from the membrane mimicking environment by collision induced dissociation (CID) in the mass spectrometer. This procedure is used to enable precise mass and ion mobility measurements of the stripped protein or protein complex.[27,28]

Here we demonstrate that near-isotropic β-barrel-like Aβ(1−42) hexamers are indeed formed and enriched upon incubation in zwitterionic phosphocholine micelles, supporting the proposed βPFO mediated membrane disruption.[22]

■ METHODS

Sample Preparation. βPFOs$_{Aβ(1−42)}$ were prepared as described previously.[22] Briefly, human recombinant Aβ(1−42) (rPeptide) was dissolved in 10 mM Tris-HCl (Amresco) pH 9.0 with PC12 as incubation detergent (Avanti Lipids) in a 1:2 peptide/micelle ratio (typically 100 μM peptide and 4.5 mM incubation detergent PC12, corresponding to 3 × CMC) and incubated under quiescent conditions at 37 °C for 24 h. After incubation, the sample was purified for analysis by size exclusion chromatography (SEC) using a Superdex 75 10/300 GL column (GE Healthcare) and a mobile phase of 10 mM ammonium acetate (Invitrogen) pH 9 with 1 mM nonionic Dodecyl Maltoside (DDM) as analysis detergent (Anatrace) (6.7 × CMC). The fractions were collected, and the secondary structure of each fraction was determined using circular dichroism (CD) spectroscopy. The fractions containing the presumed βPFOs$_{Aβ(1−42)}$-micelle complexes (larger apparent mass than the monomer and β-sheet structure) were flash frozen in liquid nitrogen and stored at −80 °C until analysis. The samples were further buffer exchanged into 200 mM ammonium acetate pH 7.5 with 0.3 mM of the analysis detergent DDM (2 × CMC) right before analysis using Micro-BioSpin P6 (Bio-Rad) columns.

Mass Spectrometry and Ion Mobility. A Waters Synapt G2S hybrid mass/ion mobility spectrometer equipped with a nano-electrospray source was used for analysis. Samples were introduced using commercial metal coated borosilicate spray emitters (Thermo Scientific). Ionization was performed in positive ion mode, and the instrument parameters were as follows: Capillary voltage 1.7 kV, Sampling cone 40 V, Source offset 80 V, Trap gas 10 mL/min, Helium Gas Flow 100 mL/min, IM gas flow 50 mL/min, IM wave velocity 750 m/s, IM wave height 24 V. CID was performed by using collisional energies between 100 and 200 V in the IM Trap region of the instrument.

Drift times from IM-MS for βPFOs$_{Aβ(1−42)}$ were calibrated to obtain CCS values as described elsewhere.[29] Human insulin (Sigma), bovine ubiquitin (Sigma), and bovine milk β-lactoglobulin (Sigma) were used as calibrants. More specifically, the insulin monomer (+3, +4), dimer (+5, +6), hexamer (+9, +11), ubiquitin monomer (+4, +5), β-lactoglobulin monomer (+7, +8, +9), and dimer (+11, +12, +13) ions were used for calibration, as they span the m/z range of Aβ(1−42) dimers to hexamers. Reference CCSs for these calibrants were obtained from published work performed on drift tube ion mobility instruments.[30,31] A calibration curve was obtained (Figure S17) with a maximum back-calculated CCS error of ±5% for the calibrant proteins.

Structure Modeling. The Aβ monomer is known to transiently fold into a β-hairpin structure in aqueous solution, which can be captured and stabilized in an affibody complex.[32] Engineered stable β-hairpin structured Aβ peptides rapidly form stable β-sheet structured oligomers that do not proceed to form amyloid fibrils.[21,33] A previous study has also found (using CD and NMR spectroscopy) that the presumed βPFOs$_{Aβ(1−42)}$ formed during the experimental conditions employed in this study have predominately β-sheet structure.[22]

The solution state NMR structure of the Aβ monomer in complex with the Z$_{Aβ3}$ affibody dimer (pdb: 2otk) was therefore selected as a reasonable building block for the βPFO model.[32] All atoms of the
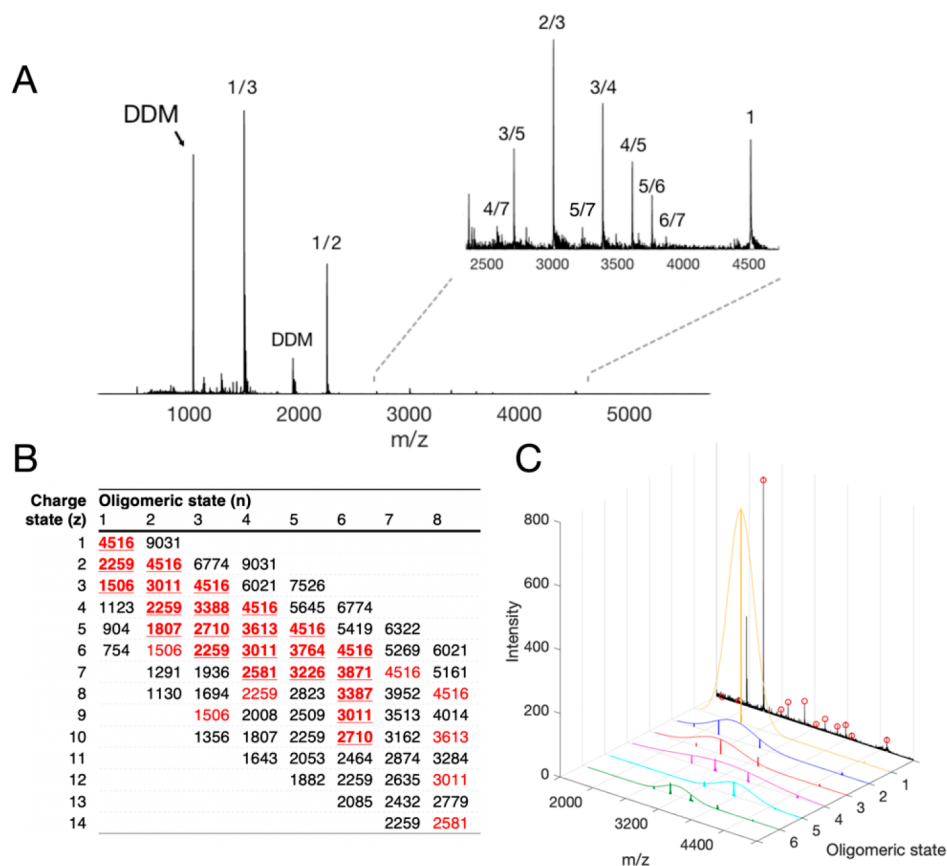
Figure 1. (A) Mass spectrum of βPFOs$_{A\beta(1-42)}$. The sample was collected from the β-sheet structured oligomer SEC fraction and buffer exchanged into 0.3 mM of the analysis detergent DDM (2 × CMC) with 200 mM ammonium acetate before analysis. Inset shows a closer look at the region where larger oligomers are expected to appear. Peaks can be observed which can be matched to theoretical Aβ(1−42) oligomeric states. The notation used is the oligomeric state divided by the charge state (n/z). Note for example that 2/3 can therefore contain dimer (+3), tetramer (+6), and hexamer (+9) components. (B) The oligomer peaks in part A have been assigned by comparing the experimentally found n/z values to the theoretically calculated n/z values. The experimentally observed states are shown in red font. It can be seen that the largest oligomer where a continuous series of charge states is observed is the hexamer. Signals confirmed by IM to correspond to a specific oligomeric state are shown in bold and underlined. (C) The fraction of each overlapping peak that correspond to a specific oligomer signal can be extracted by IM. The IM-selected MS peaks for the different oligomers together with a Gaussian fit are shown in color; the total spectrum is shown in black. The red circles in the black total spectrum indicate the total added intensity of the different deconvoluted oligomeric components, indicating that the six oligomeric components are enough to fully explain the Aβ peaks observed in the mass spectrum.

affibody dimer were removed, and the N-terminal part of another NMR model of Aβ (pdb: 1ba4[34]) was added (since the N-terminal part (1−15) of the Aβ peptide is missing from pdb 2otk due to its flexible nature in solution). The initial pdb stuctures and the final monomer model are shown in Figure S1.

Oligomeric models were constructed from this monomeric unit by *ab initio* docking using the homo-oligomer docking server GalaxyHomomer.[35] Further refinement of the docked structure was done using GalaxyRefineComplex, which uses a Monte Carlo algorithm and Molecular Dynamics simulations for relaxation and energy minimization of the docked complex.[36] The theoretical CCS values for the models were calculated using the Trajectory Method of IMPACT.[37]

■ RESULTS AND DISCUSSION

Ion mobility resolved Aβ(1−42) hexamers can be detected in the presence of micelles. Upon 24 h incubation of Aβ(1−42) with PC-12 and separation by SEC chromatography, a new peak with a higher apparent molecular weight than the Aβ(1−42) monomer appeared in the SEC chromatogram. CD spectroscopy confirmed β-sheet structure in the fraction corresponding to that peak (Figure S2). Direct analysis of this fraction eluted in 10 mM ammonium acetate

buffer with 1 mM analysis detergent. DDM resulted in a mass spectrum with major peaks from free DDM molecules or small detergent clusters. Less intense signals corresponding to Aβ monomers and small oligomers were also detectable after collisional activation and detergent dissociation (Figure S3). Significantly more intense signals were obtained after performing buffer exchange into 200 mM ammonium acetate with 0.3 mM of the analysis detergent DDM (2 × CMC) resulting in the spectrum in Figure 1A. A trap collision energy of at least 100 V was required for declustering of detergent and detection of oligomeric Aβ signals. Increased trap collision energy resulted in not only better signal-to-noise ratios but also a shift toward lower m/z values as well as drift time changes (Figure S4). These drift time shifts only occur at m/z signals containing overlapping oligomeric forms, indicating oligomer dissociation rather than unfolding events.

The signals which were coeluting in the "oligomer" SEC peak were first putatively annotated by their oligomer/charge (n/z) ratio by comparing the measured m/z values to the theoretical values for oligomers of Aβ(1−42). Theoretical oligomer m/z values are shown in Figure 1B with the experimentally observed signals marked in red. Considerable
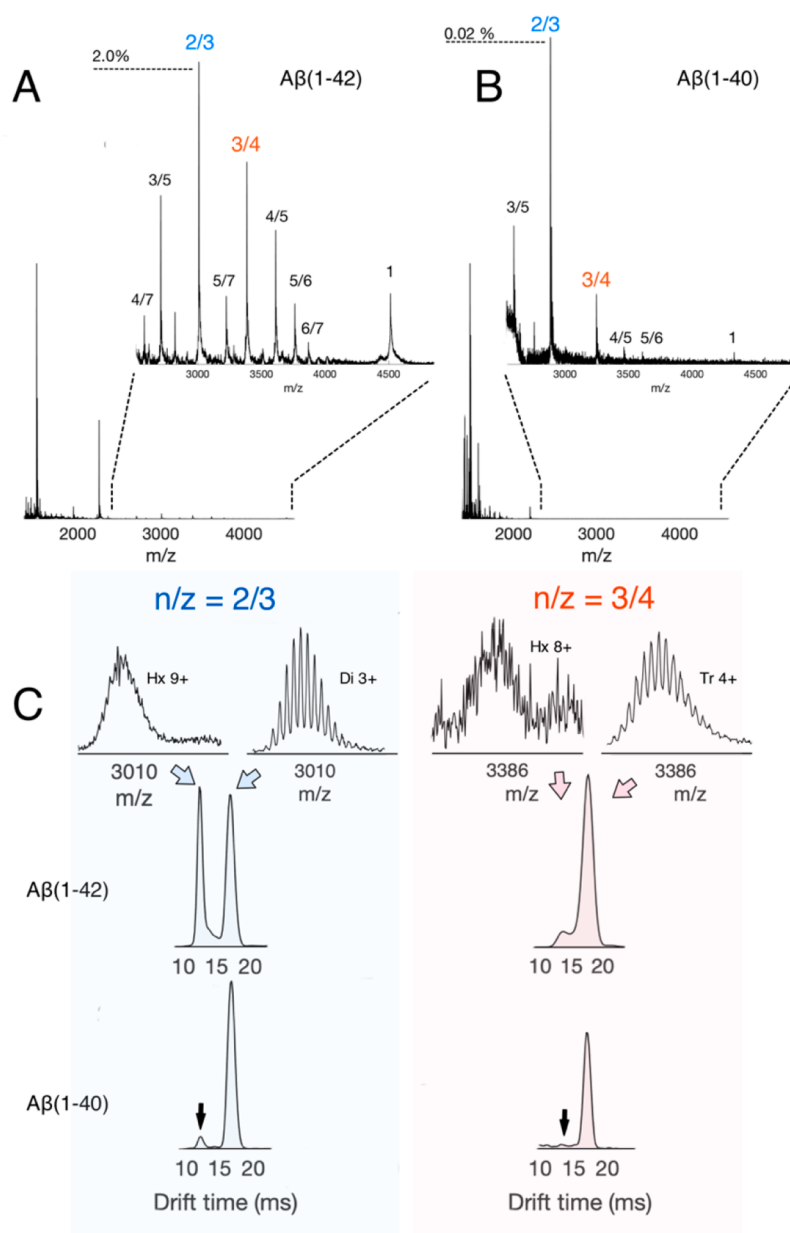
Figure 2. (A) Mass spectrum of Aβ(1−42) after 90 min of incubation in 5.5 mM DPC at 37 °C and buffer exchange to 0.3 mM DDM. The oligomeric region is shown as an insert. It can be seen that the spectrum is very similar to that from the βPFO$_{Aβ(1−42)}$ sample in Figure 1A. The intensity for the most intense oligomeric peak (2/3) is approximately 2% of the intensity of the monomeric signals. (B) Mass spectrum of Aβ(1−40) after 90 min of incubation in 5.5 mM DPC at 37 °C and buffer exchange to 0.3 mM DDM. Oligomeric signals are fewer and have lower relative intensity compared to the signals from Aβ(1−42) shown in part A. The intensity for the most intense oligomeric peak (n/z = 2/3) is only approximately 0.02% of the intensity of the monomer. (C) Drift time profiles for the n/z = 2/3 and 3/4 signals which for Aβ(1−42) contain overlapping oligomeric signals. It can be seen that the component representing the hexameric state significantly smaller for Aβ(1−40) compared to Aβ(1−42) (marked with black arrows).

overlaps of peak series are expected in the m/z dimension as n-mers can also carry n times the monomer charge. The n/z ratio is therefore a very useful notation for the experimentally observed signals (For example, the n/z = 2/3 signal could consist of a dimer (2/3), tetramer (4/6), and hexamer (6/9) component). It can be seen in Figure 1B that the hexamer is the largest oligomer where a complete series of charge states, with a Gaussian-like envelope including both even and odd charge states, was detected. The only putative heptamer signal is at n/z = 1 ("7/7") which overlaps with all other oligomers. As detected charge states in Figure 1B fall on a somewhat linear trend line (increasing the oligomeric state increases the

solvent exposed surface area, which leads to a proportional increase in average charge state), one would expect that the most intense charge state for the heptamer would be 7/8 or 7/9, neither of which are found experimentally. The potential octamer signals shown in Figure 1B are only from even charge states, which overlap heavily with signals for other smaller oligomers, making these unlikely to originate from the octamer. This indicates that the hexamer is the largest detected oligomer. As can be seen in Figure S5 the average charge state per monomer decreases for each oligomeric state. The decrease is however smaller between the tetramer and the pentamer, while the hexamer displays a slight increase in

average charge. Charging in electrospray can be explained in terms of protein conformation and accessible surface area, as is further discussed in the last part of the results section.

By taking advantage of the capability of ion mobility to deconvolute oligomer series which overlap in the m/z dimension but differ in drift time, oligomers were separated and definitively assigned using the IM dimension. The drift times for ion mobility species of overlapping n/z, which depends on charge as well as the size of the particles, were corrected by multiplication with the ion charge at a given oligomeric state. Peaks from different n/z states with approximately overlapping charge-corrected drift times were assigned to be of the same oligomeric state. This corresponds to drift time peaks of a particular oligomeric state approximately falling on a diagonal trend line in the driftogram (Figure S6). Using this simple approach most drift time peaks could be assigned to an oligomeric state. The assignment procedure is shown in Figure S7. The drift time assignment of each oligomeric n/z signal can be found in Figure S8. Higher charge states often exhibit several drift time peaks even though the n/z should not contain overlapping oligomeric states (for example 2/5, 5/7, 4/7, Figure S8). This occurrence of ions with multiple cross sections could be explained by the presence of subunit rearrangement or alternative topologies for such ions of higher charge states.[38,39]

The contributions of the individual oligomeric states to overlapping n/z signals were picked out using the IM dimension as shown in Figure 1C. All IM-filtered oligomer m/z peaks follow Gaussian shaped charge state distributions, which points toward correct IM annotation. The red circles in Figure 1C indicate the sum of intensities for the different deconvoluted oligomer components in a given n/z signal. The match between the sum of assigned components and the measured mass spectrum indicate that the monomer and six oligomer states are sufficient to fully explain the experimental data in the m/z dimension.

Aβ(1−40) form significantly lower amounts of oligomers compared to Aβ(1−42). The results from Aβ(1−42) were compared to those from Aβ(1−40). No βPFO peak of higher apparent molecular weight was observed in the SEC chromatogram for incubated Aβ(1−40), as had been reported earlier. To study the formation of oligomers we instead incubated Aβ(1−40) and Aβ(1−42) in the incubation detergent PC12 for only 90 min. The samples were then buffer exchanged into 200 mM ammonium acetate pH 9 with 0.3 mM DDM using Micro-BioSpin P6 columns and immediately analyzed in IM-MS. As can be seen in Figure 2A and B, large differences between the results from two proteoforms could be observed: Aβ(1−42) form almost identical oligomer distributions after 90 min as after 24 h. In contrast, Aβ(1−40) displayed 2 orders of magnitude lower oligomeric signals relative to the monomeric signal (with approximately the same total monomeric signal intensity) as well as fewer overall oligomer signals and an oligomeric population shifted toward lower oligomers of mostly dimers and trimers (Figure 2). Aβ(1−40) does also not exhibit a complete charge state series for the hexamer, lacking the unique $n/z = 6/7$ charge state. The ion mobility of possibly overlapping oligomers such as $n/z = 2/3$ and 3/4 also show that the ion mobility peaks annotated to the hexamer are considerably smaller than for Aβ(1−42) (Figure 2C). Aβ(1−42) could still be successfully sprayed without problem after 24 h of incubation while no spectrum could be obtained from Aβ(1−40) due to immediate clogging

of the electrospray needle, indicating heterogeneous formation of amyloid fibrils. βPFOs$_{Aβ(1−42)}$ are stable for several days in room temperature while Aβ(1−40) rapidly goes on to form amyloid fibrils without significantly populating the βPFO state after the first hours of incubation.

These results show that while oligomers are enriched in PC12 micelles for Aβ(1−42), they form at much smaller amounts for Aβ(1−40) and are of lower average oligomeric states. A minimum oligomer size is needed to create an internal cavity where leakage across a biological membrane could be facilitated. It could therefore be considered that smaller oligomers should be less toxic than larger oligomers based on the hypothesis of a pore formation−neurotoxicity connection. From our docked models of the Aβ(1−42) β-hairpin monomer, it seems like the tetramer is the smallest β-hairpin oligomer which is big enough to be able to form a proper pore structure (Figure S9). Larger oligomers are more likely to form pore structures and are therefore of increased interest for the toxicity mechanism of the peptide. This is in agreement with a structure−toxicity study which shows correlation between pore formation and toxicity for Aβ oligomers larger than the tetramer.[40]

These different behaviors in a membrane-mimicking environment, where Aβ(1−40) mostly form oligomers smaller than this critical pore formation size, could indicate a molecular background for the differences in toxicity between the Aβ(1−40) and Aβ(1−42).

The micellar environment enriches partially buried oligomers which assemble over time. More intense oligomer signals and oligomers of lower average charge are observed for the βPFOs$_{Aβ(1−42)}$ samples compared to Aβ(1−42) in a detergent-free solution (Figure S10). The charging in electrospray ionization under native conditions is typically proportional to the solvent accessible surface area of the protein.[41] The charge of micelle-embedded proteins after CID removal of detergent consequently corresponds to the charge that would be carried by a soluble protein of the same size as the soluble part of the membrane protein.[42,43] In this case, the low amount of charges per monomer is similar to the charging which has previously been observed for the hydrophilic Aβ(1−16) segment in solution.[44] The sparsely charged species that we observe therefore indicates that the peptide ions are from a micelle-bound origin, as the micelle makes some protonation sites unavailable. The N-terminal parts are most likely located outside of the micelle due to their hydrophilicity, as has been observed for the monomer in micelles.[45] These hydrophilic segments are therefore probably the regions in the βPFOs$_{Aβ(1−42)}$ which acquire the charge during the electrospray process. Similar shifts toward lower electrospray charge states have previously been observed for Aβ(1−40) monomers inserted in zwitterionic micelles, but not in the presence of nonionic micelles where the peptide is not inserted.[46] As a control experiment a peptide with the same amino acid composition as Aβ(1−42) but with a scrambled sequence (Aβ(1−42)$_{Scr}$) was used (Sequence in Supporting Information). As can be seen in Figure S11A, the hydrophobicity of Aβ(1−42)$_{Scr}$ is more equally distributed along the peptide sequence compared to Aβ(1−42). Aβ(1−42)$_{Scr}$ was treated exactly as Aβ(1−42) and was incubated in PC12 and buffer exchanged into DDM for analysis. Aβ(1−42)$_{Scr}$ monomers showed the same charge state distribution as Aβ(1−42) in a detergent-free solution even at high activation energies needed to remove the detergent. However, no oligomer signals could

be observed in Aβ(1−42)$_{Scr}$ (Figure S11B−C). Both micelle insertion and oligomer formation therefore seem to be sequence specific for the Aβ(1−42) peptide.

To further examine if the observed Aβ(1−42) oligomers are of micelle-bound origin, the sample was fractionated using an Amicon Ultra centrifugal filter (Merck) with a 30 kDa cutoff. The βPFOs$_{Aβ(1−42)}$ could still be detected in the retentate, while only monomers and oligomers of lower n/z ratio (1/4, 1/3, and 2/5) could be detected in the filtrate (Figure S12). This confirms that the observed oligomeric signals from the βPFOs$_{Aβ(1−42)}$ samples are part of larger peptide-micelle coclusters in solution, as all observed oligomers have molecular masses below 30 kDa in the absence of detergent.

The βPFOs$_{Aβ(1−42)}$ samples do also not form amyloid fibrils to the same extent as the corresponding micelle-free samples (Figure S13). Previous studies have shown that the Aβ oligomer population never reaches more than 1.5% of the total Aβ monomer concentration during amyloid aggregation studies under micelle-free in vitro conditions.[47] It would not be appropriate to use mass spectrometry data to determine the absolute quantitative oligomer concentration. However, the relative increase in oligomeric Aβ(1−42) signals upon incubation in micelles indicates an overall increase in the oligomer population compared to the micelle-free conditions. The increased oligomer population and decreased fibrillation rate at these βPFO-forming conditions therefore suggest that Aβ(1−42) oligomers can potentially be enriched in cellular membranes. Such enrichment could play an important role in AD pathology, as oligomers have a higher toxicity compared to mature amyloid fibrils.[48−50]

Increased detergent concentration at constant peptide concentration, i.e. a decrease in the theoretical peptide:micelle ratio, resulted in changes in the oligomer distribution as could be seen by IM-MS. Detergent concentrations below the formal CMC of the incubation detergent PC12 resulted in detection of predominantly hexamers at the n/z = 2/3 signal. Increasing the amount of PC12 during incubation resulted in an absolute signal increase for all oligomeric states at n/z = 2/3 (Figure 3A, top and middle panels), indicating a detergent driven oligomerization process. A relative shift toward smaller oligomers could also be observed, probably due to dilution of the peptides in the larger pool of detergent. However, if the diluted peptide−micelle mixture was incubated for a short period of time, a shift back toward larger oligomers was observed (Figure 3A, middle and lower panels), demonstrating that larger peptide oligomers assemble inside the micelles over time in an equilibrium process. The dissociation of oligomers upon dilution points toward a somewhat low stability of the structures. The reassembly however implies that the oligomers are energetically favorable compared to the state with dispersed monomers. Favorable monomer−detergent interactions could lead to an energy barrier for oligomerization, and incubation time is therefore needed to reform the complexes. The same shift toward lower oligomers at higher detergent concentration could also be observed by increasing the concentration of the DDM detergent used during analysis (Figure 3B).

Addition of PC lipids stabilizes larger oligomers. A detergent micelle is only a membrane-mimicking environment, and some caution should be taken when interpreting the results in terms of more biological contexts. The phosphocholine headgroup of the incubation detergent PC12 is a biologically relevant chemical motif, making this particular
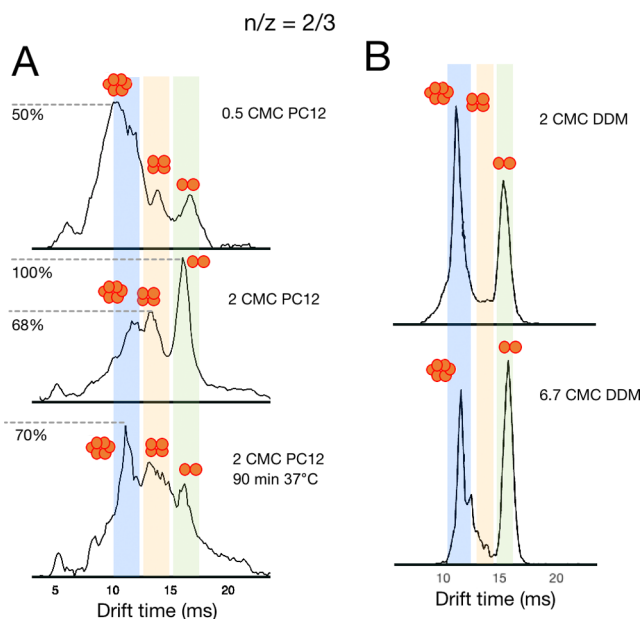
Figure 3. (A) Ion mobility drift times for Aβ(1−42) n/z = 2/3 dimers/tetramers/hexamers etc. ions with different concentrations of PC12 detergent. The relative oligomer distribution shift toward smaller species as the detergent concentration is increased (top, middle). The amount of larger oligomers is however increasing again upon incubation (middle, bottom). The relative intensities are indicated, with the most intense peak as "100%". (B) The same behavior for the n/z = 2/3 ion is observed when varying the amount of DDM detergent during analysis.

detergent reasonably relevant in a cellular context. In order to evaluate the stabilities of the βPFOs$_{Aβ(1−42)}$ in a lipid environment, the samples were titrated with a proper PC lipid (See Supporting Information), 1-palmitoyl-2-oleoyl-glycero-3-phosphocholine (POPC, 16:0−18:1 PC). Mixed micelles and bicelles are formed when lipids are added to detergent micelles, which are characterized by their [lipid]/[detergent] ratio (q-value). The βPFOs$_{Aβ(1−42)}$ were titrated with lipid to a q-value of 0.4. The oligomeric ensembles were left entirely intact as seen by their MS signals. No additional oligomeric signals were detected, but a small shift in relative intensity of the signal ensemble toward oligomers with larger n/z values could be observed (Figure S14). Ion mobility further confirms that the βPFOs$_{Aβ(1−42)}$ are shifted toward larger oligomeric states at overlapping n/z signals (Figure 4), indicating a stabilizing effect of PC lipids on the complexes. The major part of the βPFOs are detected in the unbound delipidated state, but PC binding can be observed. Ion mobility confirms the oligomeric identity of such binding events, which also further confirms the proposed IM annotation (Figure S15). It can also be seen in Figure S15 that lipid binding does not seem to alter the βPFO in a way that significantly changes the drift time of the 2/3 hexameric ion.

Other lipid classes might have different effects on stabilization or destabilization of the βPFOs$_{Aβ(1−42)}$ and could possibly also display a stronger specific binding affinity to the complexes. The herein described methodology could in the future be used to screen for such different properties.

Oligomers adopt near-isotropic β-barrel-like structures. Collisional cross section (CCS) values were determined for the experimental βPFO$_{Aβ(1−42)}$IM signals. The type of oligomer assembly can be determined by studying the CCS
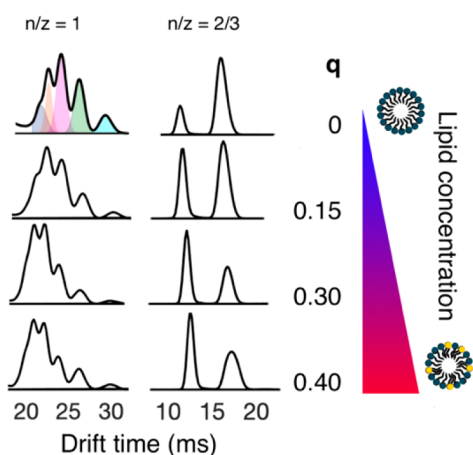
Figure 4. (A) Ion mobility drift times for Aβ(1−42) $n/z = 1$ and $n/z = 2/3$ at different [lipid]/[detergent] ratios (q-value) upon titration with 16:0−18:1 PC lipid to βPFOs$_{Aβ(1−42)}$ in DDM (0.36 mM). The relative oligomer distributions at a given n/z value shift toward larger oligomers (lower drift times) at higher q-values.

growth upon increasing oligomeric size.[51] Linear growth ($\Omega_n = \Omega_1 \cdot n$) indicates a strong spatial "1D" dependence typical of fibril assembly into roughly cylindrical structures, while isotropic growth ($\Omega_n = \Omega_1 \cdot n^{2/3}$) indicates assembly into granular "3D" aggregates. It has been found that some amyloidogenic peptides oligomerize in an isotropic manner while others grow linearly.[51] The experimentally found and the theoretically calculated CCS values assuming idealized linear and idealized isotropic growth can be seen in Figure 3A. The growth of the Aβ(1−42) oligomers clearly agrees well with isotropic growth, indicating the formation of near-spherical or

"3D" structures rather than extended linear or "1D" sheet structures.

This isotropic growth is also reflected in the average charge of the oligomeric states as seen in Figure S5. Average charge state and charge state distributions depend on the solvent accessible surface area of the protein as discussed previously, which is correlated to the CCS. It can even be argued that charge state distribution analysis gives better information on the solution state structure of proteins as electrospray charging occurs in solution while CCS values are measured on gas phase structures.[52] Information from charge states is particularly useful for unstructured proteins and protein segments.[53] Both the average charge state (Figure S5) and CCS (Figure 5) suggest that the hexamer is slightly more extended and/or solvent exposed than the simple isotropic model would suggest. This could be an indication of a structure which form a somewhat hollow pore structure, while the smaller oligomers are not large enough to do this.

The hexamer is the largest observed oligomer under these conditions. It probably also has a size that easily permits formation of hollow structures (Figure S9). Several theoretical hexamer models were constructed to compare with the experimental findings. *Ab initio* docking of the hairpin structured Aβ monomer (Figure S1) resulted in a symmetrical β-barrel structure as the best scored hexamer model from the docking. The theoretical CCS of this hexamer model was calculated to 2610 Å^2. An experimental CCS of 2100 ± 300 Å^2 (95% confidence interval) was measured for the hexamer if averaged over all charge states, this is somewhat smaller than the value for the theoretical model. This could be attributed to the fact that the unstructured N-terminal parts are very extended in the model structure. If the N-terminal parts are removed entirely, a model CCS of 1740 Å^2 is obtained, which
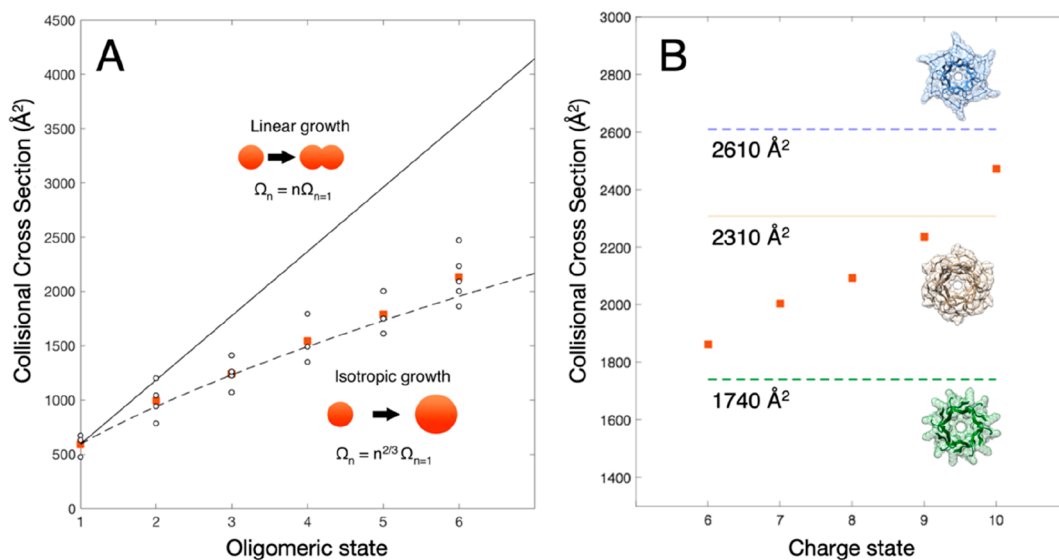
Figure 5. (A) Experimentally found CCS values for the βPFOs$_{Aβ(1−42)}$. The determined CCS values for each charge state are given in the open circles while the red squares represent the average CCS over all charge states for a given oligomeric state. The calculated (equations shown in figure) theoretical CCS values for ideal linear and isotropic growth of the measured monomer CCS are plotted in solid and dashed lines, respectively. It can be seen that the data for Aβ(1−42) are in very good agreement with the isotropic growth model. (B) Calculated CCS values for theoretical models of an Aβ hexamer built using *ab initio* docking are shown by the horizontal lines. The blue structure is the structure given by the docking program. The tan structure represents a refined version of the blue structure where the energy has been minimized by Monte Carlo/Molecular Dynamics simulation. The green structure is the blue structure without the N-terminal (1−16) part. The red boxes show the experimentally found CCS values for the Aβ(1−42) hexamer for each charge state. The results show that N-terminal extendedness and/or orientation could explain the charge dependent changes in CCS.

is slightly smaller than the most compact charge state observed. The observed CCS values for the oligomers increase by around 10% for each added charge (Figure 3B). As most charges should be located in the N-terminal segments, a charge−charge repulsion driven expansion is expected in these parts of the molecules, as has been reported for the isolated Aβ(1−16) segment.[44] This reasoning agrees with the observation that the experimental CCS values lie between the CCS of the N-terminal free model and the CCS of the model where the N-terminal parts are largely extended and are protruding outward from the center (Figure 3B). Refinement of the *ab initio* docking model by the Web server GalaxyRefineComplex where the structure has been allowed to relax and reach an energy minimum does indeed yield a structure with a slightly smaller CCS of 2310 Å^2, which agrees better with the measured values. This model value is also close to the CCS of the experimentally highly populated +9 charge state (2236 Å^2) (Figure 3B).

As mentioned above this hexamer model is big enough to easily form a pore-like structure with a hollow channel in the middle of the oligomer. It also seems likely that the opening and internal cavity of this modeled β-barrel hexamer structure is big enough (8.9 Å at the narrowest point) for ions to transverse the membrane through this channel. In Figure 6A the internal cavity of the top scored β-barrel structure is shown together with a divalent calcium ion (green) at the narrowest point of the channel. Figure 6A also shows that the height of

the oligomeric peptide complex roughly agrees with the bilayer thickness of a typical lipid membrane.

Other symmetric hexameric structures were also constructed for comparison, including tilted hexameric barrels, star shaped hexamers, dimers of trimers, and trimers of dimers. These are summarized in Figure S16. The experimental CCS range can then be used to filter out modeled structures which are significantly different from the measured values. The barrel-like structures (the proper symmetric barrels described above, as well as a compact trimer of dimers which is also a barrel-like structure) were the most compact structures as well as the only structures with CCS values within the experimental measured CCS range (Figure 6B). No models had CCS values in agreement with the smallest CCS values determined from IM-MS. It is well-known that protein structures, particularly hollow ones, often collapse slightly in the gas phase, forming more compact folds due to increased electrostatic interactions.[38] Gas phase collapse could therefore yield experimental structures which are slightly more compact than the models obtained from docking. It has recently been reported that Aβ oligomers undergo a slight shift in secondary structure toward helical structure in the most hydrophobic segments upon transfer to the gas phase.[54] A hexamer formed from docking of helical Aβ peptides (pdb: 2lfm[55]) gives a similar CCS (2560 Å^2) as the β-barrel structures. This illustrates the limitation of CCS in distinguishing between different secondary structure elements. The CCS value should rather be seen to inform about the overall oligomer symmetry and size.

CONCLUDING REMARKS

Native mass spectrometry was used to detect the formation of Aβ(1−42)β-barrel pore forming oligomers ($\beta PFOs_{A\beta(1-42)}$) and to describe their exact oligomeric states. These oligomeric structures, which could represent some of the most neurotoxic Aβ species, are difficult to study using other techniques, as the Aβ population is very heterogeneous. The $\beta PFOs_{A\beta(1-42)}$ are furthermore associated with detergent molecules, making the exact oligomer sizes difficult to determine in solution. As mass spectrometry is a nonaveraging technique, it is possible to separately detect all species present in the sample. It is also possible to strip the peptide−micelle complexes down to pure peptide oligomers with distinct masses by carefully applying collisional energy in the mass spectrometer.

In the β-sheet structured size exclusion chromatography fraction, we could confidently detect oligomer sizes up to hexamers. The spread in oligomer sizes further illustrates the heterogeneity of the peptide population also in a somewhat stabilizing membrane-mimicking environment. Oligomers larger than tetramers are probably big enough to form pore structures and therefore warrant special attention. Such potentially pore-forming oligomers were exclusively observed for Aβ(1−42), while Aβ(1−40) mostly formed dimers and trimers. No heptamers or octamers could be detected even at low collisional energies, which could possibly indicate that the hexamer is the largest oligomeric state in this particular system. The importance of the hexamer in the oligomerization pathway for Aβ(1−42) in solution has previously been demonstrated.[6] It has however been envisioned that the hexamers go on to form the so-called Aβ(1−42) globulomer (60−100 kDa oligomer found in solution), consisting of two stacked hexamers with the hydrophobic C-terminal ends of both hexamers at the center of the structure.[6,56] The fact that we do

Figure 6. (A) Illustration of the best scored docked hexamer structure (symmetric β-barrel) with the width of the internal channel indicated at the narrowest and widest points. A Ca^{2+} ion is shown for comparison (green) inside the channel. The height of the hexamer is approximately the same as the thickness of the DPPC (PC 16:0) bilayer shown in gray (carbon atoms)/red (oxygen atoms). (B) Overview of the calculated CCS values for some of the oligomer structures obtained from *ab initio* docking. The experimentally observed CCS mean with 95% confidence interval is shown by the red line. Some representative structures of Aβ hexamer models are shown. Compact barrel-like structures are the models which best agree with the experimental data.

not observe such dodecamers could be explained by stabilization (solvation) of the C-termini by hydrophobic detergent hydrocarbon tails in our system. Such solvation would remove the entropic drive for dimerization of hexamers present in an aqueous solution. This could be an artifact of the micelle model, but similar stabilizing effects would likely be present also in a lipid bilayer.

We furthermore show that the smaller oligomers assemble into larger oligomers upon incubation and that addition of PC lipids to the micelles stabilizes larger oligomers. The hexamer was the largest observed oligomers under all tested conditions. The decrease of fibrillation rate in combination with an increase in oligomer population indicates the potentially important role of membranes in $A\beta$ mediated neurotoxicity. βPFOs could represent an alternative population state for the $A\beta$-peptide which is highly neurotoxic and possibly not on-pathway for amyloid formation. The observed difference between βPFO-formation for $A\beta(1-42)$ and $A\beta(1-40)$ furthermore gives a connection between intrinsic peptide toxicity and their corresponding ability to form pore-like structures in membranes.

The experimentally obtained collisional cross section values for the βPFOs are in good agreement both with isotropic growth and with a theoretical β-barrel model built using *ab initio* docking. Alternative oligomer symmetries are all significantly larger than the cross sections obtained experimentally. Our results therefore prove that oligomeric $A\beta$ structures are formed and enriched under conditions that have been shown to induce membrane leakage,[22] supporting the idea of neurotoxic membrane-bound $A\beta$ pores. The hexameric βPFOs$_{A\beta(1-42)}$ described here has many features in common with the crystal structure of a hexamer formed by a segment of the amyloid-forming protein of αB crystalin (cylindrin).[57] It was, in the same study, bioinformatically predicted that the C-terminal part of the $A\beta$-peptide should also be able to form such a cylindrin-like hexamer structure. Theoretical MD models have additionally been presented of hexameric $A\beta(1-42)$ pores in a PC lipid bilayer.[58] Such pores, which our results now give experimental proof for, could be a highly relevant part of the pathological mechanism in AD, which of course in a physiological context could be even more complex.

The methodology presented here could be further applied to study how different specific lipids could stabilize or destabilize certain oligomeric forms of the βPFOs, as has been shown recently for other membrane proteins.[59] It is possible that certain conditions could decrease the heterogeneity and increase the relative concentration of pore-forming (tetramers and larger) oligomers. Specifically, it is known that anionic lipids, gangliosides, and cholesterol could influence the $A\beta-$membrane interaction.[60–63] $A\beta$ sequence variations or modifications such as disease related mutants or oxidation induced covalent cross-linking could also be factors that cause increased stability of βPFOs and increased neurotoxicity. βPFOs are interesting potential key players in neurodegeneration and could therefore be interesting as potential targets for future AD therapies. More generally the approach presented here could also be applied to other similar targets, as it is hypothesized by some that many amyloidogenic peptides and proteins oligomerize and disturb membranes in similar ways.[64] Pore formation is also a debated topic within the fields of cell-penetrating and antimicrobial peptides.[65,66] Our results show that native ion mobility mass spectrometry is very useful and

an important tool for studies of peptide oligomerization also in the membrane environment.

■ ASSOCIATED CONTENT

ⓢ Supporting Information

The Supporting Information is available free of charge on the ACS Publications website at DOI: 10.1021/jacs.9b04596.

Additional experimental details and supporting figures (PDF)

■ AUTHOR INFORMATION

Corresponding Authors

*astrid.graslund@dbb.su.se
*f.sobott@leeds.ac.uk

ORCID

Nicklas Österlund: 0000-0003-0905-7911
Leopold L. Ilag: 0000-0003-3678-7100

Notes

The authors declare no competing financial interest.

■ REFERENCES

(1) Chow, V. W.; Mattson, M. P.; Wong, P. C.; Gleichmann, M. An Overview of APP Processing Enzymes and Products. *NeuroMol. Med.* **2010**, *12*, 1–12.

(2) Selkoe, D. J.; Hardy, J. The Amyloid Hypothesis of Alzheimer's Disease at 25 Years. *EMBO Mol. Med.* **2016**, *8* (6), 595–608.

(3) McLean, C. A.; Cherny, R. A.; Fraser, F. W.; Fuller, S. J.; Smith, M. J.; Vbeyreuther, K.; Bush, A. I.; Masters, C. L. Soluble Pool of $A\beta$ Amyloid as a Determinant of Severity of Neurodegeneration in Alzheimer's Disease. *Ann. Neurol.* **1999**, *46* (6), 860–866.

(4) Lin, H. A. I.; Bhatia, R.; Lal, R. Amyloid β Protein Forms Ion Channels: Implications for Alzheimer's Disease Pathophysiology. *FASEB J.* **2001**, *15* (13), 2433–2444.

(5) Lashuel, H. A.; Lansbury, P. T. Are Amyloid Diseases Caused by Protein Aggregates That Mimic Bacterial Pore-Forming Toxins? *Q. Rev. Biophys.* **2006**, *39*, 167–201.

(6) Bernstein, S. L.; Dupuis, N. F.; Lazo, N. D.; Wyttenbach, T.; Condron, M. M.; Bitan, G.; Teplow, D. B.; Shea, J. E.; Ruotolo, B. T.; Robinson, C. V.; Bowers, M. T. Amyloid-β Protein Oligomerization and the Importance of Tetramers and Dodecamers in the Aetiology of Alzheimer's Disease. *Nat. Chem.* **2009**, *1* (4), 326–331.

(7) Meisl, G.; Yang, X.; Hellstrand, E.; Frohm, B.; Kirkegaard, J. B.; Cohen, S. I. A.; Dobson, C. M.; Linse, S.; Knowles, T. P. J. Differences in Nucleation Behavior Underlie the Contrasting Aggregation Kinetics of the $A\beta40$ and $A\beta42$ Peptides. *Proc. Natl. Acad. Sci. U. S. A.* **2014**, *111* (26), 9384–9389.

(8) Bode, D. C.; Baker, M. D.; Viles, J. H. Ion Channel Formation by Amyloid-$\beta42$ Oligomers but Not Amyloid-$\beta40$ in Cellular Membranes. *J. Biol. Chem.* **2017**, *292* (4), 1404–1413.

(9) Bokvist, M.; Lindström, F.; Watts, A.; Gröbner, G. Two Types of Alzheimer's β-Amyloid (1–40) Peptide Membrane Interactions: Aggregation Preventing Transmembrane Anchoring Versus Accelerated Surface Fibril Formation. *J. Mol. Biol.* **2004**, *335* (4), 1039–1049.

(10) Relini, A.; Marano, N.; Gliozzi, A. Probing the Interplay between Amyloidogenic Proteins and Membranes Using Lipid

Monolayers and Bilayers. *Adv. Colloid Interface Sci.* **2014**, *207* (1), 81−92.

(11) Khondker, A.; Alsop, R. J.; Rheinstädter, M. C. Membrane-Accelerated Amyloid-*β* Aggregation and Formation of Cross-*β* Sheets. *Membranes* **2017**, *7* (3), 49.

(12) Devanathan, S.; Salamon, Z.; Lindblom, G.; Gröbner, G.; Tollin, G. Effects of Sphingomyelin, Cholesterol and Zinc Ions on the Binding, Insertion and Aggregation of the Amyloid A*β*1−40 Peptide in Solid-Supported Lipid Bilayers. *FEBS J.* **2006**, *273* (7), 1389−1402.

(13) Sciacca, M. F. M.; Kotler, S. A.; Brender, J. R.; Chen, J.; Lee, D. K.; Ramamoorthy, A. Two-Step Mechanism of Membrane Disruption by A*β* through Membrane Fragmentation and Pore Formation. *Biophys. J.* **2012**, *103* (4), 702−710.

(14) Sciacca, M. F. M.; Brender, J. R.; Lee, D. K.; Ramamoorthy, A. Phosphatidylethanolamine Enhances Amyloid Fiber-Dependent Membrane Fragmentation. *Biochemistry* **2012**, *51* (39), 7676−7684.

(15) Korshavn, K. J.; Satriano, C.; Lin, Y.; Zhang, R.; Dulchavsky, M.; Bhunia, A.; Ivanova, M. I.; Lee, Y. H.; La Rosa, C.; Lim, M. H.; Ramamoorthy, A. Reduced Lipid Bilayer Thickness Regulates the Aggregation and Cytotoxicity of Amyloid-*β*. *J. Biol. Chem.* **2017**, *292* (11), 4638−4650.

(16) Österlund, N.; Luo, J.; Wärmländer, S. K. T. S.; Gräslund, A. Membrane-Mimetic Systems for Biophysical Studies of the Amyloid-*β* Peptide. *Biochim. Biophys. Acta, Proteins Proteomics* **2019**, *1867* (5), 492.

(17) Tiiman, A.; Jarvet, J.; Gräslund, A.; Vukojevic, V. Heterogeneity and Intermediates Turnover during Amyloid-*β* (A*β*) Peptide Aggregation Studied by Fluorescence Correlation Spectroscopy. *Biochemistry* **2015**, *54* (49), 7203−7211.

(18) Abelein, A.; Kaspersen, J. D.; Nielsen, S. B.; Jensen, G. V.; Christiansen, G.; Pedersen, J. S.; Danielsson, J.; Otzen, D. E.; Gräslund, A. Formation of Dynamic Soluble Surfactant-Induced Amyloid *β* Peptide Aggregation Intermediates. *J. Biol. Chem.* **2013**, *288* (32), 23518−23528.

(19) Kreutzer, A. G.; Nowick, J. S. Elucidating the Structures of Amyloid Oligomers with Macrocyclic *β*-Hairpin Peptides: Insights into Alzheimer's Disease and Other Amyloid Diseases. *Acc. Chem. Res.* **2018**, *51* (3), 706−718.

(20) Kotler, S. A.; Brender, J. R.; Vivekanandan, S.; Suzuki, Y.; Yamamoto, K.; Monette, M.; Krishnamoorthy, J.; Walsh, P.; Cauble, M.; Holl, M. M. B.; Marsh, E. N. G; Ramamoorthy, A. High-Resolution NMR Characterization of Low Abundance Oligomers of Amyloid-*β* without Purification. *Sci. Rep.* **2015**, *5*, DOI: 10.1038/srep11811.

(21) Sandberg, A.; Luheshi, L. M.; Sollvander, S.; Pereira de Barros, T.; Macao, B.; Knowles, T. P. J.; Biverstal, H.; Lendel, C.; Ekholm-Petterson, F.; Dubnovitsky, A.; Lannfelt, L.; Dobson, C. M.; Härd, T. Stabilization of Neurotoxic Alzheimer Amyloid-*β* Oligomers by Protein Engineering. *Proc. Natl. Acad. Sci. U. S. A.* **2010**, *107* (35), 15595−15600.

(22) Serra-Batiste, M.; Ninot-Pedrosa, M.; Bayoumi, M.; Gairí, M.; Maglia, G.; Carulla, N. A*β*42 Assembles into Specific *β*-Barrel Pore-Forming Oligomers in Membrane-Mimicking Environments. *Proc. Natl. Acad. Sci. U. S. A.* **2016**, *113* (39), 10866−10871.

(23) Marcoux, J.; Robinson, C. V. Twenty Years of Gas Phase Structural Biology. *Structure* **2013**, *21*, 1541−1550.

(24) Ilag, L. L.; Ubarretxena-Belandia, I.; Tate, C. G.; Robinson, C. V. Drug Binding Revealed by Tandem Mass Spectrometry of a Protein-Micelle Complex. *J. Am. Chem. Soc.* **2004**, *126* (44), 14362−14363.

(25) Marty, M. T.; Zhang, H.; Cui, W.; Blankenship, R. E.; Gross, M. L.; Sligar, S. G. Native Mass Spectrometry Characterization of Intact Nanodisc Lipoprotein Complexes. *Anal. Chem.* **2012**, *84* (21), 8957−8960.

(26) Marty, M. T.; Hoi, K. K.; Robinson, C. V. Interfacing Membrane Mimetics with Mass Spectrometry. *Acc. Chem. Res.* **2016**, *49* (11), 2459−2467.

(27) Barrera, N. P.; Di Bartolo, N.; Booth, P. J.; Robinson, C. V. Micelles Protect Membrane Complexes from Solution to Vacuum. *Science (Washington, DC, U. S.)* **2008**, *321* (5886), 243−246.

(28) Konijnenberg, A.; Yilmaz, D.; Ingólfsson, H. I.; Dimitrova, A.; Marrink, S. J.; Li, Z.; Vénien-Bryan, C.; Sobott, F.; Koçer, A. Global Structural Changes of an Ion Channel during Its Gating Are Followed by Ion Mobility Mass Spectrometry. *Proc. Natl. Acad. Sci. U. S. A.* **2014**, *111* (48), 17170−17175.

(29) Ruotolo, B. T.; Benesch, J. L. P.; Sandercock, A. M.; Hyung, S. J.; Robinson, C. V. Ion Mobility-Mass Spectrometry Analysis of Large Protein Complexes. *Nat. Protoc.* **2008**, *3* (7), 1139−1152.

(30) Bush, M. F.; Hall, Z.; Giles, K.; Hoyes, J.; Robinson, C. V.; Ruotolo, B. T. Collision Cross Sections of Proteins and Their Complexes: A Calibration Framework and Database for Gas-Phase Structural Biology. *Anal. Chem.* **2010**, *82* (22), 9557−9565.

(31) Salbo, R.; Bush, M. F.; Naver, H.; Campuzano, I.; Robinson, C. V.; Pettersson, I.; Jørgensen, T. J. D.; Haselmann, K. F. Traveling-Wave Ion Mobility Mass Spectrometry of Protein Complexes: Accurate Calibrated Collision Cross-Sections of Human Insulin Oligomers. *Rapid Commun. Mass Spectrom.* **2012**, *26* (10), 1181−1193.

(32) Hoyer, W.; Gronwall, C.; Jonsson, A.; Stahl, S.; Hard, T. Stabilization of a Beta-Hairpin in Monomeric Alzheimer's Amyloid-Beta Peptide Inhibits Amyloid Formation. *Proc. Natl. Acad. Sci. U. S. A.* **2008**, *105* (13), 5099−5104.

(33) Lendel, C.; Bjerring, M.; Dubnovitsky, A.; Kelly, R. T.; Filippov, A.; Antzutkin, O. N.; Nielsen, N. C.; Härd, T. A Hexameric Peptide Barrel as Building Block of Amyloid-*β* Protofibrils. *Angew. Chem., Int. Ed.* **2014**, *53* (47), 12756−12760.

(34) Coles, M.; Bicknell, W.; Watson, R. A.; Fairlie, D. P.; Craik, D. J. Solution Structure of Amyloid *β*-peptide(1−40) in a Water-Micelle Environment. Is the Membrane-Spanning Domain Where We Think It Is? *Biochemistry* **1998**, *37* (31), 11064−11077.

(35) Baek, M.; Park, T.; Heo, L.; Park, C.; Seok, C. GalaxyHomomer: A Web Server for Protein Homo-Oligomer Structure Prediction from a Monomer Sequence or Structure. *Nucleic Acids Res.* **2017**, *45* (W1), W320−W324.

(36) Heo, L.; Lee, H.; Seok, C. GalaxyRefineComplex: Refinement of Protein-Protein Complex Model Structures Driven by Interface Repacking. *Sci. Rep.* **2016**, *6*, DOI: 10.1038/srep32153.

(37) Marklund, E. G.; Degiacomi, M. T.; Robinson, C. V.; Baldwin, A. J.; Benesch, J. L. P. Collision Cross Sections for Structural Proteomics. *Structure* **2015**, *23* (4), 791−799.

(38) Breuker, K.; McLafferty, F. W. Stepwise Evolution of Protein Native Structure with Electrospray into the Gas Phase, 10−12 to 102 S. *Proc. Natl. Acad. Sci. U. S. A.* **2008**, *105* (47), 18145−18152.

(39) Meyer, T.; Gabelica, V.; Grubmüller, H.; Orozco, M. Proteins in the Gas Phase. *Wiley Interdiscip. Rev. Comput. Mol. Sci.* **2013**, *3* (4), 408−425.

(40) Prangkio, P.; Yusko, E. C.; Sept, D.; Yang, J.; Mayer, M. Multivariate Analyses of Amyloid-Beta Oligomer Populations Indicate a Connection between Pore Formation and Cytotoxicity. *PLoS One* **2012**, *7* (10), e47261.

(41) Testa, L.; Brocca, S.; Grandori, R. Charge-Surface Correlation in Electrospray Ionization of Folded and Unfolded Proteins. *Anal. Chem.* **2011**, *83* (17), 6459−6463.

(42) Barrera, N. P.; Zhou, M.; Robinson, C. V. The Role of Lipids in Defining Membrane Protein Interactions: Insights from Mass Spectrometry. *Trends Cell Biol.* **2013**, *23*, 1−8.

(43) Allison, T. M.; Landreh, M.; Benesch, J. L. P.; Robinson, C. V. Low Charge and Reduced Mobility of Membrane Protein Complexes Has Implications for Calibration of Collision Cross Section Measurements. *Anal. Chem.* **2016**, *88* (11), 5879−5884.

(44) Li, J.; Lyu, W.; Rossetti, G.; Konijnenberg, A.; Natalello, A.; Ippoliti, E.; Orozco, M.; Sobott, F.; Grandori, R.; Carloni, P. Proton Dynamics in Protein Mass Spectrometry. *J. Phys. Chem. Lett.* **2017**, *8* (6), 1105−1112.

(45) Jarvet, J.; Danielsson, J.; Damberg, P.; Oleszczuk, M.; Gräslund, A. Positioning of the Alzheimer A*β*(1−40) Peptide in SDS Micelles

Using NMR and Paramagnetic Probes. *J. Biomol. NMR* **2007**, *39* (1), 63–72.

(46) Österlund, N.; Kulkarni, Y. S.; Misiaszek, A. D.; Wallin, C.; Krüger, D. M.; Liao, Q.; Mashayekhy Rad, F.; Jarvet, J.; Strodel, B.; Wärmländer, S. K. T. S.; Ilag, L. L.; Kamerlin, S. C. L.; Gräslund, A. Amyloid-β Peptide Interactions with Amphiphilic Surfactants: Electrostatic and Hydrophobic Effects. *ACS Chem. Neurosci.* **2018**, *9* (7), 1680–1692.

(47) Linse, S. Monomer-Dependent Secondary Nucleation in Amyloid Formation. *Biophys. Rev.* **2017**, *9*, 329–338.

(48) Sengupta, U.; Nilson, A. N.; Kayed, R. The Role of Amyloid-β Oligomers in Toxicity, Propagation, and Immunotherapy. *EBio Medicine.* **2016**, *6*, 42–49.

(49) Viola, K. L.; Klein, W. L. Amyloid β Oligomers in Alzheimer's Disease Pathogenesis, Treatment, and Diagnosis. *Acta Neuropathol.* **2015**, *129*, 183–206.

(50) Mroczko, B.; Groblewska, M.; Litman-Zawadzka, A.; Kornhuber, J.; Lewczuk, P. Amyloid β Oligomers (AβOs) in Alzheimer's Disease. *Journal of Neural Transmission.* **2018**, *125*, 177–191.

(51) Bleiholder, C.; Dupuis, N. F.; Wyttenbach, T.; Bowers, M. T. Ion Mobilityg-Mass Spectrometry Reveals a Conformational Conversion from Random Assembly to β-Sheet in Amyloid Fibril Formation. *Nat. Chem.* **2011**, *3* (2), 172–177.

(52) Grandori, R. Origin of the Conformation Dependence of Protein Charge-State Distributions in Electrospray Ionization Mass Spectrometry. *J. Mass Spectrom.* **2003**, *38*, 11–15.

(53) Vahidi, S.; Stocks, B. B.; Konermann, L. Partially Disordered Proteins Studied by Ion Mobility-Mass Spectrometry: Implications for the Preservation of Solution Phase Structure in the Gas Phase. *Anal. Chem.* **2013**, *85* (21), 10471–10478.

(54) Liu, L.; Dong, X.; Liu, Y.; Österlund, N.; Gräslund, A.; Carloni, P.; Li, J. Role of Hydrophobic Residues for the Gaseous Formation of Helical Motifs. *Chem. Commun.* **2019**, *55* (35), 5147–5150.

(55) Vivekanandan, S.; Brender, J. R.; Lee, S. Y.; Ramamoorthy, A. A Partially Folded Structure of Amyloid-beta(1–40) in an Aqueous Environment. *Biochem. Biophys. Res. Commun.* **2011**, *411* (2), 312–316.

(56) Barghorn, S.; Nimmrich, V.; Striebinger, A.; Krantz, G.; Keller, P.; Janson, B.; Bahr, M.; Schmidt, M.; Bitner, R. S.; Harlan, J.; Barlow, E.; Ebert, U.; Hillen, H. Globular Amyloid β-peptide1−42oligomer - A Homogenous and Stable Neuropathological Protein in Alzheimer's Disease. *J. Neurochem.* **2005**, *95* (3), 834–847.

(57) Laganowsky, A.; Liu, C.; Sawaya, M. R.; Whitelegge, J. P.; Park, J.; Zhao, M.; Pensalfini, A.; Soriaga, A. B.; Landau, M.; Teng, P. K.; Cascio, D.; Glabe, C.; Eisenberg, D. Atomic View of a Toxic Amyloid Small Oligomer. *Science (Washington, DC, U. S.)* **2012**, *335* (6073), 1228–1231.

(58) Strodel, B.; Lee, J. W. L.; Whittleston, C. S.; Wales, D. J. Transmembrane Structures for Alzheimer's Aβ1−42 Oligomers. *J. Am. Chem. Soc.* **2010**, *132* (38), 13300–13312.

(59) Landreh, M.; Marklund, E. G.; Uzdavinys, P.; Degiacomi, M. T.; Coincon, M.; Gault, J.; Gupta, K.; Liko, I.; Benesch, J. L. P.; Drew, D.; Robinson, C. V. Integrating Mass Spectrometry with MD Simulations Reveals the Role of Lipids in Na+/H+antiporters. *Nat. Commun.* **2017**, *8*, 13993.

(60) Kakio, A.; Nishimoto, S. I.; Yanagisawa, K.; Kozutsumi, Y.; Matsuzaki, K. Cholesterol-Dependent Formation of GM1 Ganglioside-Bound Amyloid β-Protein, an Endogenous Seed for Alzheimer Amyloid. *J. Biol. Chem.* **2001**, *276* (27), 24985–24990.

(61) Nakazawa, Y.; Suzuki, Y.; Williamson, M. P.; Saitô, H.; Asakura, T. The Interaction of Amyloid Abeta(1−40) with Lipid Bilayers and Ganglioside as Studied by 31P Solid-State NMR. *Chem. Phys. Lipids* **2009**, *158*, 54.

(62) Ahyayauch, H.; Raab, M.; Busto, J. V.; Andraka, N.; Arrondo, J. L. R.; Masserini, M.; Tvaroska, I.; Goñi, F. M. Binding of β-Amyloid (1−42) Peptide to Negatively Charged Phospholipid Membranes in the Liquid-Ordered State: Modeling and Experimental Studies. *Biophys. J.* **2012**, *103* (3), 453–463.

(63) Fantini, J.; Di Scala, C.; Yahi, N.; Troadec, J. D.; Sadelli, K.; Chahinian, H.; Garmy, N. Bexarotene Blocks Calcium-Permeable Ion Channels Formed by Neurotoxic Alzheimer's β-Amyloid Peptides. *ACS Chem. Neurosci.* **2014**, *5* (3), 216–224.

(64) Quist, A.; Doudevski, I.; Lin, H.; Azimova, R.; Ng, D.; Frangione, B.; Kagan, B.; Ghiso, J.; Lal, R. Amyloid Ion Channels: A Common Structural Link for Protein-Misfolding Disease. *Proc. Natl. Acad. Sci. U. S. A.* **2005**, *102* (30), 10427–10432.

(65) Nguyen, L. T.; Haney, E. F.; Vogel, H. J. The Expanding Scope of Antimicrobial Peptide Structures and Their Modes of Action. *Trends Biotechnol.* **2011**, *29*, 464–472.

(66) Bechara, C.; Sagan, S. Cell-Penetrating Peptides: 20 Years Later, Where Do We Stand? *FEBS Lett.* **2013**, *587*, 1693–1702.